Proceeding of the 15th ME-NETT conference

A Decoupled Electrical–Thermal and Mechanical Model for Resistance Spot Welding

C. SRIKUNWONG†, T. DUPUY†† and Y. BIENVENU†††
†Student, Ecole des Mines de Paris, BP 87, Evry Cedex 91003, Paris, France
††Usinor R&D, USINOR Group, CRDM, BP 2508, 59381, Dunkerque Cedex 1, France
†††Professor, Ecole des Mines de Paris, BP 87, Evry Cedex 91003, Paris, France

Abstract

Resistance spot welding is one of the major joining methods used in automotive body fabrication and assembly. It is well known that resistance spot welding is a very complex process. In order to profoundly understand the interactions among the electrical-thermal and mechanical aspects and simulate the physical phenomena of resistance spot welding, a 2-D axisymmetric finite element model with the decoupled electro-thermal and mechanical analyses for resistance spot welding was developed by employing a commercial finite element code, namely, SYSWELD. The assumptions introduced to the model : the Joule heating at the workpiece and the electrode interface, the latent heat of phase change due to melting was taken into account by utilizing the electro-thermal enthalpy model. The interfaces between the electrode-to-sheet and sheet-to-sheet contact were specially treated with artificial interface elements. Force and current were considered as principal welding parameters. A parametric study is carried out for the nugget growth with specific consideration of resistance spot welding of a similar non-coating sheet assembly.

In addition, the electro-thermal contact resistances, mechanical contact models as well as material properties and characteristics were described as temperature-dependent functions throughout the study. During nugget formation stages, it was evidently disclosed that Joule heating at long welding times governs the nugget growth and heat generation at the faying surface dominates the nugget formation.

The influence of thermal contact model definition and size on nugget formation, thermal history and thermal-caused stress distributions in the assembly was determined. The mechanical - thermal analysis for the squeeze and weld stages were also investigated for each case of welding forces imposed to the model. Therefore, the influence of welding force on the stress distributions can be determined, especially for the squeeze phase of resistance spot welding.

1. Introduction

Resistance spot welding is widely applied in manufacturing industries for joining similar as well as dissimilar metal sheets. The major advantages of resistance spot welding are the followings :

1) High productivity : the time for one cycle of total RSW phases is less than one second.
2) Low cost : the conventional copper electrode can be easily utilized and replaced.
3) Wide range of applications for complex geometry and material combinations, especially for the automotive industry.
4) No mass added : suitable for light-weight structure.
5) Compatibility to automatic welding, controlling and monitoring processes.
6) Clean process : no slag occurring at the welding joint.

In resistance spot welding, the high current intensity flow and heat generation are localized at the weld point which is predetermined by the design of the electrode. In many applications of the automotive industries, the flat tip electrode is used as well as the curved tip electrode. Resistance spot welding process involves the interactions of electrical, thermal, mechanical and metallurgical phenomena. Concerning any assembly of sheets and electrode used, the principal parameters of resistance spot welding are welding current, force and duration of welding cycle. All parameters of resistance spot welding are strongly interrelated and lead to the determination of the weld lobe, which is a diagram used to determine the welding range for a certain type of sheet assembly. In order to determine the process parameters, to design electrodes or to choose the type and capacity of the welding machine while developing a new process in industry, a great number of running-in experiments have often to be undertaken. These increase the cost of products, time and in many cases delay the onset of production. For the above reasons, the application of computer simulation using numerical methods may save time and decrease cost-spent on the development of product or process, and moreover reveal a more detailed information of the internal phenomena and thus facilitating a better understanding of the processes. In the present study, the numerical simulation modelling of the resistance spot welding process is carried out by using the commercial finite element code SYSWELD®.

After the first remarkable work in finite element method for resistance spot welding of Nied [Ref.1] in 1984, FEM has been recognized as a powerful tool and effectively used to obtain a better understanding in RSW process. One of the chief features of the finite element techniques is the way curved boundaries can be realistically treated by using higher order isoparametric elements. Accurate solutions can be obtained in the region where the gradients are steep by refining the mesh.

Nied utilized commercial finite element code ANSYS and introduced a quarter axisymmetric model that accounted for the geometry of electrode and workpiece, the temperature-dependent properties and characteristics of materials. The melting and Joule heating effect were also included in the model. Predictions of the electrode and the workpiece deformations as well as the stress distributions along the interface were illustrated. The thermal analysis results showed that the isotherm forms in an elliptic nugget.

In 1990, Dickinson *et al.*, [Ref. 2], modeled the RSW process by using the ANSYS finite element code. The mechanical behavior of the welding process was coupled with transient thermal response during the entire welding cycle. The weld nugget formations in 347 stainless steel of equal and unequal sheet thickness and also joining 347 stainless steel to AISI 1045 steel workpiece were studied. The FEM analysis showed that the initial heat affected zone forms as a toroid shape and spreads rapidly toward the nugget center. This phenomena had also been reported in the work of Nied. For dissimilar material, the nugget forms in the low conductivity workpiece more than in the workpiece with higher thermal conductivity. For the unequal thickness sheet, the nugget forms mostly in the thicker workpiece due to longer current path. This study provided a comprehensive information about a coupled model for analyzing the interactions of various physical phenomena in resistance spot welding.

In 1991, Tsai *et al.*, [Ref. 3], studied the nugget formation and corresponding electrode displacement during the welding cycle. They proposed that the electrode displacement and its velocity can be used as the controlling parameters in a feedback control process monitoring. Tsai reported that the heat zone initiates at the periphery of the contact area and is in a toroid shape. In a very short time during the welding cycles, the molten nugget spreads rapidly inward toward the weld center.

In 1992, Vogler *et al.*, [Ref.4], studied the temperature history in RSW from the electrical-thermal-mechanical finite element models. The electrical contact size at the faying interface was predetermined by the mechanical analysis at the end of squeeze stage and maintained throughout the electro-thermal analysis. It revealed that the presence of electrical contact resistance affects the thermal history experienced in the assembly and the final nugget diameter. However, the influence of the electrical contact size variation on the thermal history and the nugget development was not addressed in their study.

Recently, Xu *et al.*, [Refs. 5-6], modeled and simulated the resistance spot welding process using ABAQUS code. An axisymmetric finite element model employing coupled mechanical-electrical-thermal model was presented. The latent heat of phase transformation was accounted for. A flat tip electrode and sinusoidal alternating current were utilized in the analysis. An electro-thermal element was introduced to the electrode-to-sheet interface. It revealed that heat transfer coefficient of the interface has a great influence on the nugget formation and thermal distribution in the workpiece. They also reported that the contact pressure distribution at the interface during the welding process depends on the temperature history, applied force, electrode shape, friction coefficient of the interface and most importantly on the temperature-dependent material properties.

In the aforementioned documentation, it is evident that the electro-thermal and mechanical decoupling of resistance spot welding has not been well addressed yet. In order to obtain a better understanding in the influence of RSW parameters, the decoupling of electro-thermal and mechanical aspects is introduced in the present study. A fully coupled electro-thermal model results the electrical current density, electrical field, temperature history, and nugget size and geometry The thermal history obtained from the electro-thermal model will be used as thermal input data for the mechanical analysis at each considered time-step. The contact resistances of both electrode-to-sheet and sheet-to-sheet interfaces are treated with the artificial contact elements [Ref. 7] and the temperature-dependent properties and characteristics are given from various sources [Refs. 8-9]. Electrical and thermal resistances at the electrode-to-sheet and faying interfaces are described as functions of temperature based on the experimental work of [Ref. 8]. The influence of electro-thermal contact size at the faying interface on the thermal and stress results will be investigated by the variation of the faying interface diameter. The mechanical analysis provides the stress fields as well as the deformations, thus the contact stresses at the interface of both sheet-to-sheet and electrode-to-sheet can be determined.

2. Formulation for Modelling

A representative assembly of electrode and sheet utilized for analysis is shown in fig. 1. Fig. 2 illustrates a half axisymmetric finite element model for electrode and sheet assen C_L /hich is considered for both electro-thermal and ..... nical analyses.

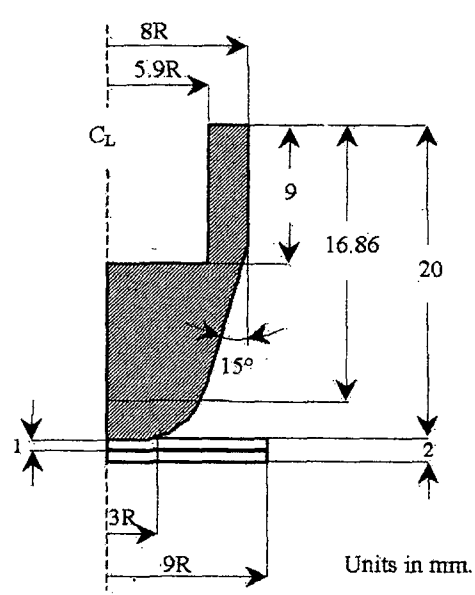

Fig. 1 Schematic diagram of RSW assembly

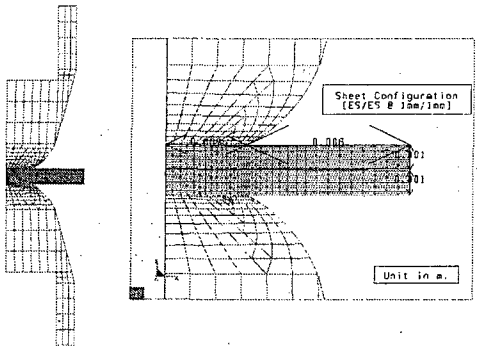

Fig. 2 Finite element mesh model

Electro-Thermal Modelling

The thermal model includes the electrode geometry, applied current, Joule heating effect at the interface, interface heat transfer coefficient and enthalpy associated with phase transformation of sheet material. Temperature-dependent thermal and electrical properties are employed in the present study. Some examples of these properties are presented in fig. 3.

Before the beginning of welding cycle, the electrical initial conditions are set equal to zero, while the temperature of entire structure is specified as the room temperature. During the welding cycle, the AC current is applied at the top of the upper electrode and zero potential is specified at the bottom surface of the lower electrode. Consequently, the current flows from the upper electrode, passes through workpiece and terminates at the bottom annular section of the lower electrode. The electro-thermal boundary conditions imposed at the outer surfaces of both electrode and workpiece are air convection for where the surface temperature being equivalent to that of the ambient and radiation heat transfer mechanism for the considerable elevated surface-temperature. Fig. 4 illustrates the imposed electro-thermal boundary conditions.

(a)

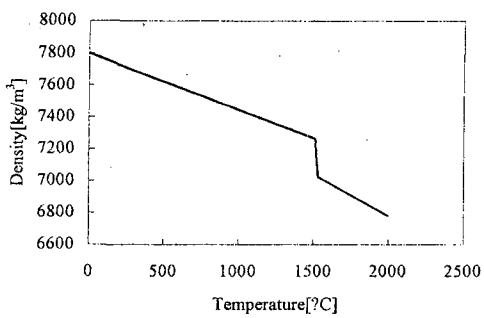

(b)

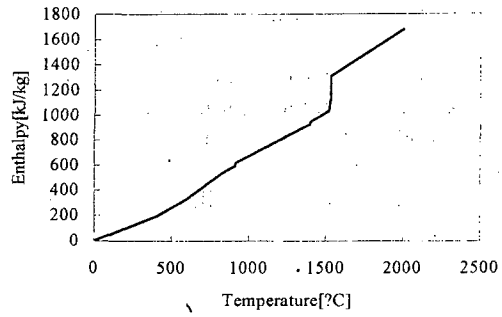

(c)

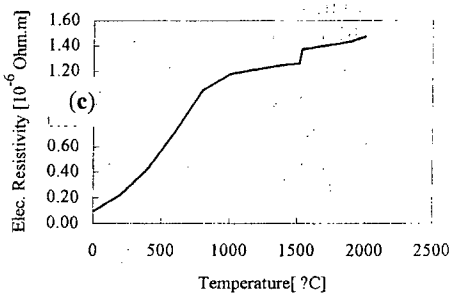

Fig. 3 Properties and characteristics of steel sheet described as a function of temperature
(a) Density
(b) Enthalpy
(c) Electrical resistivity

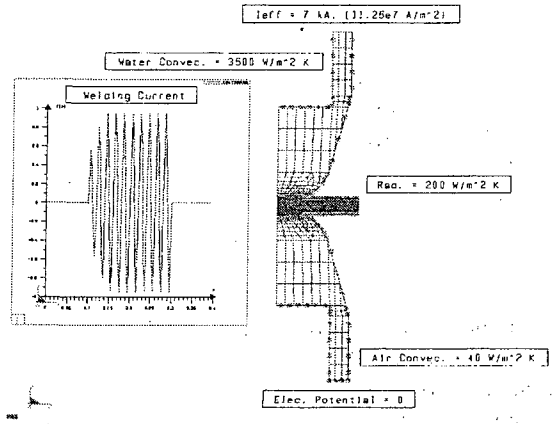

Fig. 4 Electro-thermal boundary conditions

Mechanical Modelling

The electrode force is applied since the beginning of the squeeze cycle until the end of the welding cycle. The mechanical boundary conditions imposed are the electrode force applied at the top surface of upper electrode by assuming a pressure distribution across the annular end, and the lower electrode annular section experienced the constrained condition by fixing the axial nodal displacement in y-direction. The radial nodal displacement of both workpiece and electrode are restricted along the entire axial axis corresponding to an axisymmetric boundary condition. The mechanical

boundary conditions introduced to the model simulate the restrained boundary conditions experienced from producing a welding point by the pedestal welding machine.

The mechanical properties of electrode and sheet are described as the temperature-dependent functions. Some mechanical characteristics of sheet are presented in fig. 5. Fig. 6 illustrates the mechanical boundary conditions imposed to the structure.

(a)

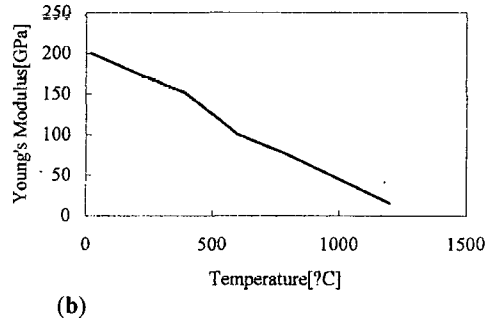

(b)

(b)

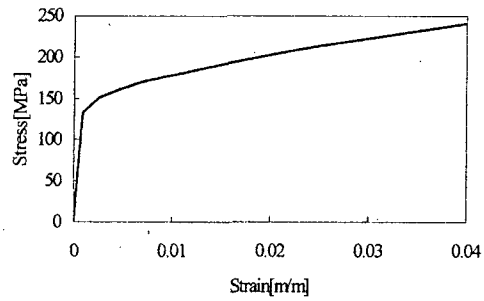

Fig. 5 Temperature-dependent mechanical characteristics of sheet material
(a) Young's modulus
(b) Stress-strain relationship at room temperature

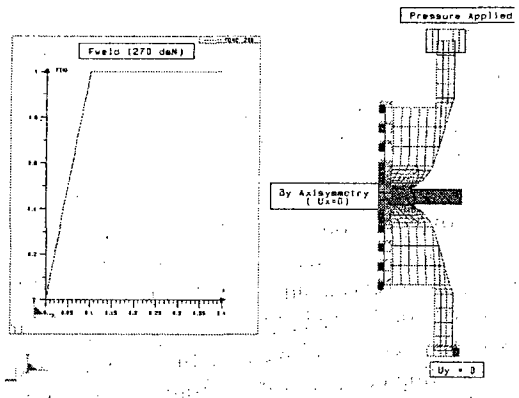

Fig. 6 Mechanical boundary conditions

Material Properties and Welding Schedule

Sheet material used in the analysis is drawing quality non-coating sheet, which is one of USINOR sheet products. Both sheets have the same thickness. Isotropic temperature-dependent properties and characteristics are specified for the electro-thermal as well as mechanical analyses. These properties are considered over a temperature ranging from room temperature to that above melting point. Material characteristics and properties introduced to the model can be concluded as the followings :

-Isotropic sheet material characteristics and properties.

-Temperature-dependent function described for both properties and mechanical characteristics of sheet, electrode as well as contact element.

A conventional copper electrode is employed and the welding schedule considered in present study is provided from [Ref. 10] corresponding to the practice. Welding conditions for non-coating sheet assembly are summarized as the followings :

Current	7.0-10.2 kA. [~AC. 50 Hz]
Welding force	250-320 daN.
Squeezing time	5 cycles. [0.1 second]
Welding time	10 cycles. [0.2 second]

According to process simulation, only the squeezing and welding phases are presented, since they are vital for the determination of the contact pressure distribution and the predicted nugget geometry.

3. Results and Discussion

Electro-Thermal Modelling

For this investigation, a welding cycle analysis is conducted to determine the current density and the temperature history experienced in the assembly and the nugget size and shape.

In order to determine the welding range from the simulation, the acceptable nugget diameter considered from the practice ranging from 4.0 to 6.0 mm. is taken into account as the weldability reference. The isotherms defined the nugget and HAZ sizes correspond to the fusion (1500 °C) and the austenitic (800 °C) temperatures, respectively.

The welding range and the variation of weld nugget geometry with current at the end of the 10th cycle resulted from simulation are shown in fig. 7. It shows that the effective current should be used is 9.35 kA. with 10 welding cycles in order to obtain the nugget diameter equal to 6 mm. In addition, the current range varied from 7.25 to 9.35 kA. provides an acceptable nugget size ranging from 4.0 to 6.0 mm.

The electro-thermal analysis reveals that the characteristic isothermal of an elliptic-shape weld nugget is always obtained at the end of welding phase as shown in fig. 7(a). Fig. 7(b) illustrates the nugget diameter size as a function of welding current. Increasing in the welding current will also increase the nugget diameter. The weld nugget is generated by the Joule heating effect occurring at the faying interface and this generation dominates the nugget formation development.

(a)

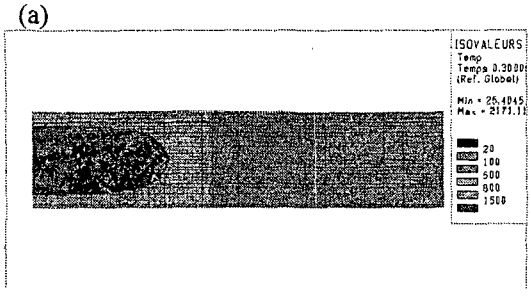

(b)

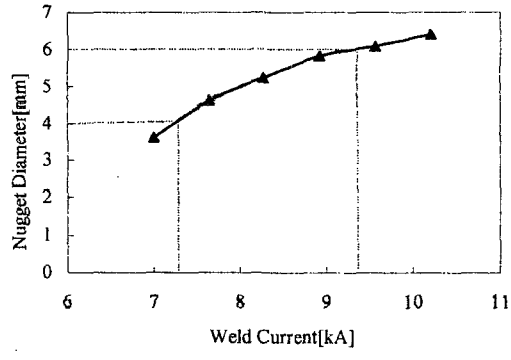

(c)

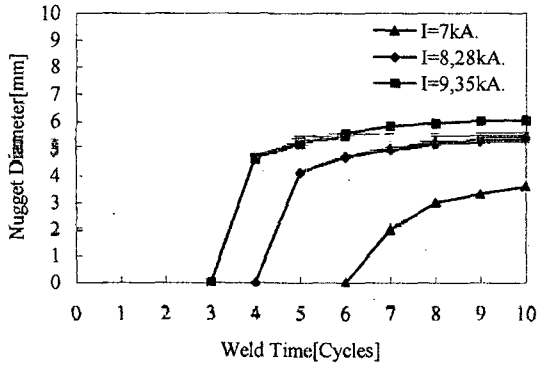

(d)

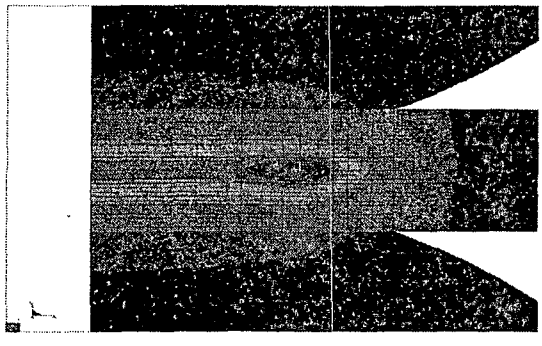

(e)

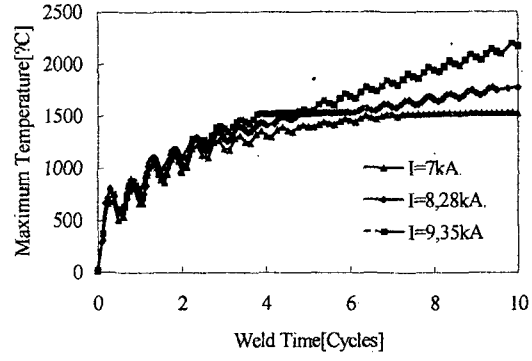

(f)

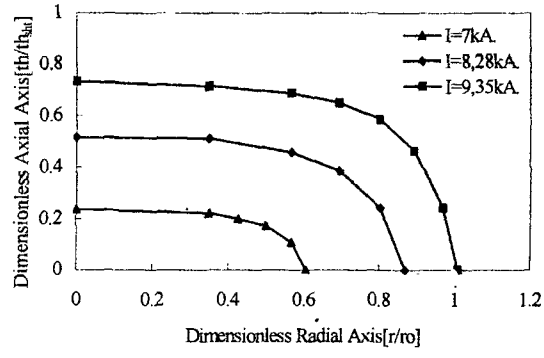

Fig. 7 Effect of welding current on nugget size and thermal history experienced in the workpiece

(a) Elliptic nugget geometry at the end of welding cycle. (case I=9.35kA)
(b) Predicted nugget diameters as a function of welding current at the end of the 10th cycle and the welding range resulted from simulation.
(c) Predicted nugget diameter evolutions as function of welding time.
(d) Early heat zone as a toroid shape occurs at the faying interface. (case I=9.35kA@ the end of the 2nd cycle)
(e) Maximum temperatures occurring at the nugget center as function of welding time for considered welding currents.
(f) Dimensionless nugget geometry variation with the welding current at the end of welding.

It is well known that only the electro-thermal model can provide an elliptic geometry of nugget. This nugget formation has been observed since the first RSW thermal analysis of Greenwood [Ref. 11]. Comparison of nugget diameter prediction and welding time is presented in fig. 7(c) for welding currents varied from 7 to 9.35 kA. It reveals that the higher welding current is applied, the earlier nugget forms in the shorter welding cycles. The nugget diameter development almost saturates after the 7th cycle and the 8th cycle for the welding currents equal to 9.35 and 8.28 kA., respectively. It is noted that the nugget starts forming about the fourth cycle for the welding current equal to 9.35 kA.

Fig. 7(d) shows the an early toroid heat zone initiates at the periphery of sheet-to-sheet interface at the end of the second welding cycle. According to the flat tip electrode used in simulation, the singularity of current occurs at this interface of contact and this generates the heat affected zone at the periphery of the contact during the welding stage. Shortly after that, the heat affected zone becomes the molten nugget, which spreads rapidly inward toward the nugget center. There is very little nugget growth in the outward radial direction. Fig. 8(b) supports this discussion after the fourth cycle in case of 9.35 kA. applied.

The maximum temperature of the weld center experienced in the workpiece for each case of welding current is illustrated in fig.7(e). It is obvious that the increase in welding current will result in higher maximum temperature reached at the weld center. It can be observed that there are slightly differences in maximum temperature history reached at the nugget center for the early welding stages and these differences in temperature increase significantly after the nugget center thermal cycle reaches the fusion state. In case of the welding current 9.35 kA., the maximum temperature cycle reaches the fusion temperature of sheet material at the end of the fourth cycle and increases markedly after the fifth cycle. The higher current applied, the more rapidly increases in the maximum temperature at the nugget center. However, these are strongly dependent on the electrode tip shape used in the simulation as described elsewhere [Ref. 12].

Fig. 7(f) depicts the dimensionless nugget geometry for the different cases of welding current. As expected, the increase in current also increases both height and diameter of nugget. Therefore, the current is considered as one of the important parameters in RSW process.

Temperature distribution along the faying surface as function of welding time is illustrated in fig. 8(a). It can be seen that the maximum temperature occurs near the periphery of sheet-to-sheet interface at the second welding cycle due to the fact that the current singularity induces the first heat affected zone at this region. In addition, the temperature distribution can be characterized as bell shape. The considerable drop in temperature can be also observed near the outer rim of the contact during the welding cycle. Fig. 8(b) reveals that the nugget develops more rapidly in the axial direction than that in the radial direction as the welding cycle increases concerning the flat tip electrode used in the simulation. In the case of current equal to 9.35 kA, the molten nugget forms firstly at the 4^{th} cycle and increases in both diameter and height during latter welding stages.

Fig. 9 shows the influence of electro-thermal contact size at the sheet-to-sheet interface on the thermal history and the nugget size. As expected, the increase in the contact size results in the decrease of the maximum temperature reached at the end of welding as well as the final nugget size. The difference in temperature at the end of welding phase comparing the thermal contact size equal to electrode diameter to that equal to one hundred and forty percents of electrode diameter is 196 °C as shown in fig. 9(a). The temperatures are slightly higher for the larger thermal contact size in the early stages of welding, in contrast to the end of welding phase, the maximum temperature profile is higher in case of smaller contact size. It has been shown that the thermal contact size influences the final nugget size as illustrated in fig. 9 (b). The increase in electro-thermal contact size at sheet-to-sheet will directly reduce the nugget size.

(a)

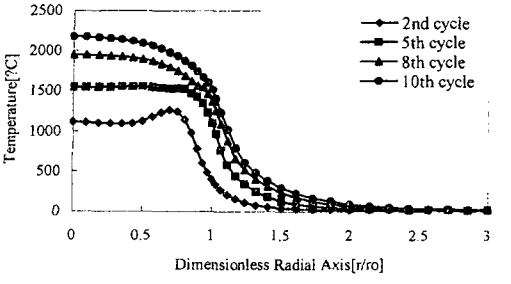

(b)

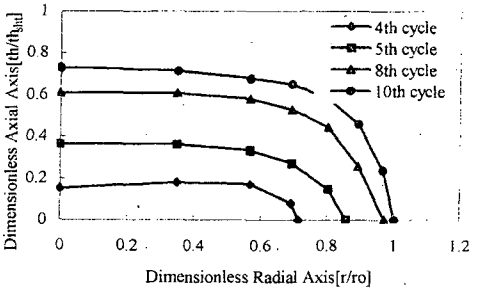

Fig. 8 Effect of welding time on thermal history and nugget size in the assembly (I=9.35 kA.)
(a) Thermal history experienced along the faying surface.
(b) Dimensionless nugget geometry vs. welding time.

(a)

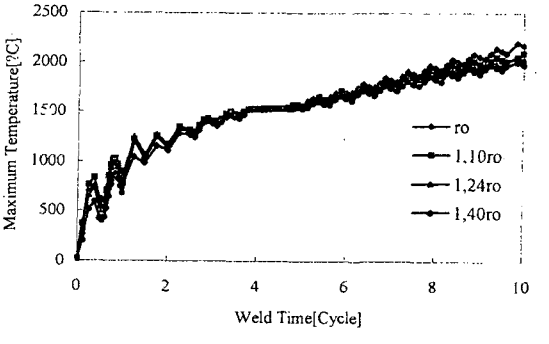

(b)

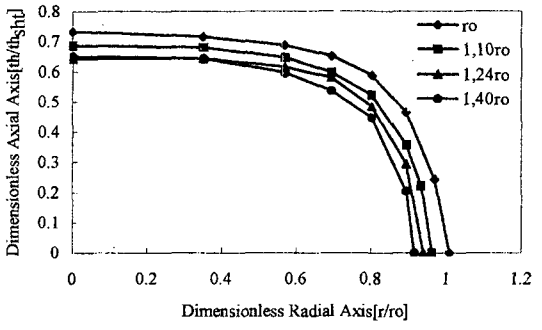

Fig. 9 Effect of thermal contact size on thermal history at nugget center and final nugget size (I=9.35 kA.)
(a) Thermal history evolution at nugget center.
(b) Dimensionless nugget geometry for different size of thermal contact at the end of welding.

Mechanical Modelling

The mechanical analysis determines the contact stress occurring at both sheet-to-sheet and electrode-to-sheet interfaces as well as the assembly deformation for the squeeze phase. The contact pressure distributions along the electrode-to-sheet and sheet-to-sheet interfaces are illustrated in fig. 10 for the squeeze phase with the various welding forces. The results indicate that once the squeeze force increases, the contact pressure also increases for both electrode-to-sheet and sheet-to-sheet interfaces. As expected, maximum contact stresses are found at the outer rim of the electrode-to-sheet interface while maximum normal stress of workpiece faying surface occurs near the periphery of contact region. The comparison of contact pressure at the end of squeeze phase reveals that the interface stress is not uniformly distributed for each case of squeeze force applied, it starts from a lower value at the axial axis and increases gradually in the radial direction of the assembly for the faying interface. The considerable drop in contact pressure can be seen at the periphery region for the faying interface. These stress concentrations at the periphery, especially for the faying interface, have a pitching effect, which can prevent molten metal of the nugget volume from the splashing.

Fig. 11 shows the predicted electrode-to-sheet contact pressure distributions for the applied force equal to 270 daN associated with various welding cycles. The results indicate that maximum pressure concentration occurs initially at the outer rim of the electrode face after the squeeze phase. When the welding current is switched on, the pressure for the center portion of electrode-to-sheet interface is noticeably shifted from 50 to 150 MPa. during the first three cycles. This instantaneous increase in the interface contact stress only occurs in the early welding stages. In the latter welding stages, in contrast to the beginning of weld, contact pressure decreases gradually for the inner-center portion of electrode-to-sheet interface while the stress concentration can be observed at the outer rim of electrode-to-sheet interface.

This contact stress concentration varies during the welding cycle and its maximum appears at the fifth cycle.

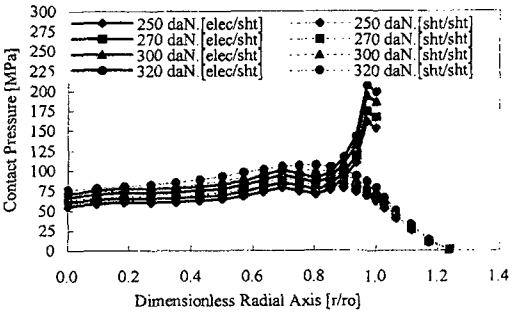

Fig. 10 Comparison of contact pressure at the end of squeezing phase for various welding forces applied

Although their model employed the coupled electrical-thermal-mechanical analysis, [Ref. 13] also reported the similar contact pressure distribution to that obtained from the present study. The combined effects of the plastic deformation due to the stress concentration at the electrode face periphery and the thermal deformation can probably cause the pitting effect at the electrode face, thus establishing the electrode degradation in the applications.

The comparison of Von-Mises stresses on electrode-to-sheet interface at the end of squeeze phase in case of different welding forces is illustrated in fig. 12. The Von-Mises stress distributions at the electrode-to-sheet interface exhibit the same manner as that of axial contact stress. Maximum Von-Mises stress occurs at the periphery of the interface and drops drastically for the region, which is no contact interface between electrode-to-sheet. During the welding cycle, the Von-Mises stress at the end of the third cycle for the inner portion of the interface due to the thermal expansion of the assembly during the welding

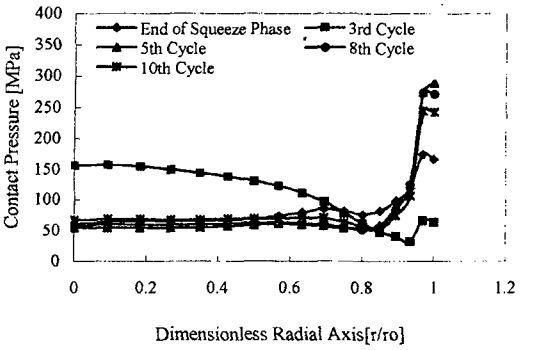

Fig. 11 Pressure distribution at electrode/sheet interface (I=9.35 kA. and F=270 daN)

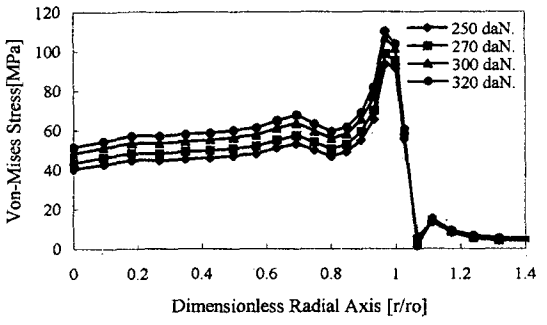

Fig. 12 Comparison of Von-Mises stress at electrode/ sheet interface for the end of squeeze phase

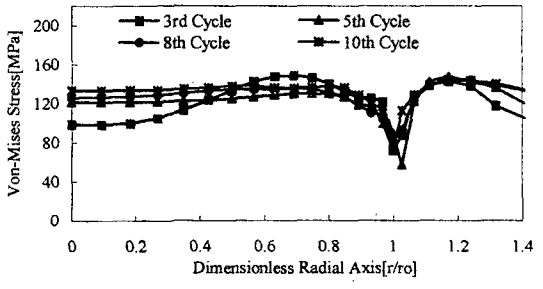

Fig. 13 Comparison of Von-Mises stress at electrode/sheet interface during welding phase (I = 9.35 kA. and F=270 daN)

phase and a significant drop in the Von-Mises stress profile can be seen at the outer rim of the contact as shown in fig. 13. The Von-Mises stress evolutions and the edge separation of the assembly during the welding phase are illustrated in fig. 14.

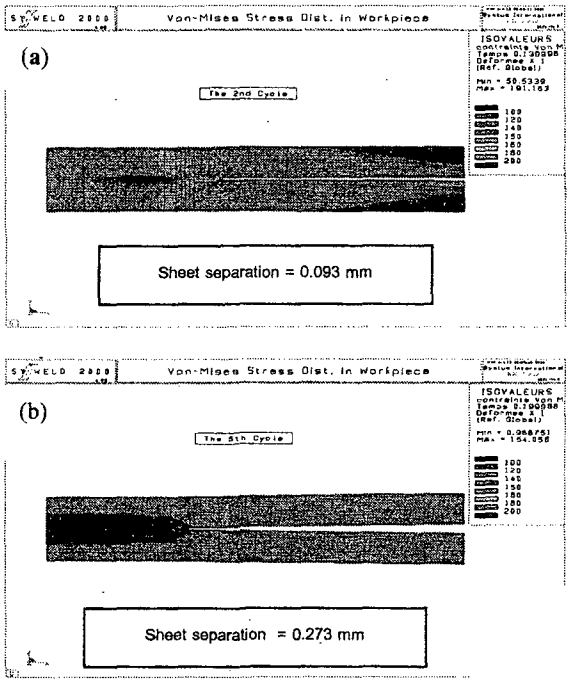

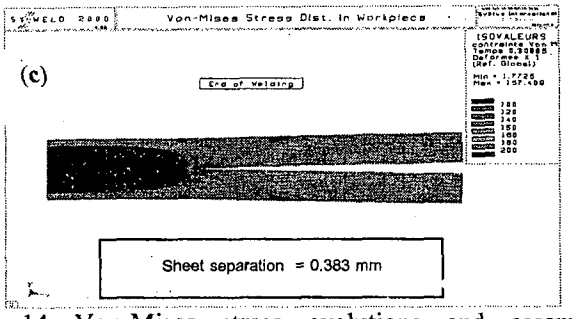

Fig.14 Von-Mises stress evolutions and assembly deformations during the welding phase
(I=9.35 kA. and F=270 daN)
(a) @ second cycle
(b) @ fifth cycle
(c) @ end of welding

4. Conclusions and Future Work

The Finite element method with the present of decoupling among electro-thermal and mechanical aspects has been developed and provided a better understanding of the internal phenomena of RSW process including the nugget development, the thermal distributions and variations, as well as the interface stress distributions during the squeezing and the welding phases.

The conclusions for the present study can be drawn as the followings :

1. It was demonstrated that the electro-thermal contact size introduced to the faying surface dominates an important role not only on the final nugget size but also on the thermal history experienced in the workpiece. The first HAZ initiates at the periphery of the faying contact and forms as toroid shape in the early stages of welding due to the current singularity. The HAZ grows rapidly inward and toward the axial axis and it becomes the nugget in the latter stages. This is the case of flat face electrode used. The acceptable nugget diameters found from the practice were employed as the weldability references compared to the simulation results, thus the electro-thermal model can provide the quantitative welding lobe.

2. A contact pressure concentration for the electrode-to-sheet interface always occurs at the interface periphery and increases with the increase of the welding force applied. Contact pressure profiles for both electrode-to-sheet and faying interfaces are not uniformly distributed at the end of squeeze as well as during welding phases.

3. The temperature-dependent properties and characteristics for both electrode and sheet must necessarily be taken into account to the model in order to obtain more accurate simulation results. Therefore, the properties and the characteristics of sheet material will be experimentally investigated and introduced to the electro-thermal and mechanical coupled model, which will consider the RSW process with the applications of both flat and curved tip electrodes producing the spot weld.

4. The coupling among the electro-thermal and mechanical aspects is important in order to construct a

model approaching more realistically to the RSW process. In addition, the experimental validations for the on-going work have to be established in order to prove the consistency of the simulation and provide the limitation of the model.

5. Acknowledgements

The authors would like to express their grateful acknowledgement to Mr. G. RIGAUT, the director of the Metallurgical Development and Research Center of SOLLAC Atlantique, Dunkerque, for his authorisation to prepare these papers as well as tremendous support.

Mr. J. CLAEYS, the head of resistance welding section, and Mr O. DIERAERT, the formerly head of resistance welding section, are gratefully acknowledged for their support.

6. References

[1] Nied, H.A., *1984*, The finite element modelling of the resistance spot welding process, *Welding journal* 63(4) : pp. 123s to 132s.

[2] Dickinson, D.W., Tsai, C.L. and Jammal, O., *Feb.26-Mar2. 1990*, Modelling of RSW nugget growth-application for the automotive industry, *International congress and exposition*, Detroit, Michigan.

[3] Tsai, C.L., Dai, W.L., Dickinson, D.W. and Papritan, J.C., *Dec.1991*, Analysis and development of a real-time control methodology in resistance spot welding, *Welding journal* : pp. 339s to 357s.

[4] Vogler, M.M., and Sheppard, S.D., *June 1-5 1992*, A study of temperature histories in resistance spot welding, *International trend in welding science and technology*, Proceedings of the 3rd int. conference on trends in welding research, Gatlinburg Tennessee, ASM : pp. 57 to 61.

[5] Xu, L. and Khan, J.A., *June 1998*, Finite element modelling of axisymmetric nugget development during resistance spot welding, *Trends in welding research* : pp. 616 to 621.

[6] Khan, J.A., Xu, L. and Chao, Y.J., *1999*, Prediction of nugget development during resistance spot welding using coupled thermal-electrical-mechanical model, *Sciences and technology of welding and joining*, Vol. 4 No.4 : pp. 201 to 207.

[7] SYSTUS® 2000, *Analysis reference manuals*, Vols. 1-4, *Edition 2000*, ESI group.

[8] Thiéblemont, E., *1992*, Modèlisation du soudage par points, *Ph.D. dissertation*, L'Institut National Polytechnique de Lorraine.(in French)

[9] Metals handbook (Desk edition) the 8th Edition, *1995*, *American society for metals*

[10] Caractérisation de la soudabilité par résistance par point de produits plats revêtus ou non, *Déc. 1994*, *Normalisation française A87-001.*

[11] Greenwood, J.A., *1961*, Temperature in spot welding, *British welding journal* : pp. 316 to 322.

[12] Murakawa, H., Kimura, F. and Ueda, Y., *the 1st edition 1997*, Weldability analysis of spot welding on aluminium using FEM, *Mathematical modelling of weld phenomena 3* : pp. 944 to 966.

[13] Dong, P., Victor Li, M. and Kimchi, M., *1998*, Finite element analysis of electrode wear mechnisms : face extrusion and pitting effects, *Science and technology of welding and joining*, Vol. 3, N°2. : pp. 59 to 64.